On the Effectiveness of OTFS for Joint Radar Parameter Estimation and Communication

# On the Effectiveness of OTFS for Joint Radar Parameter Estimation and Communication

Lorenzo Gaudio[1], Mari Kobayashi[2], Giuseppe Caire[3], and Giulio Colavolpe[1]

***Abstract*—We consider a joint radar parameter estimation and communication system using orthogonal time frequency space (OTFS) modulation. The scenario is motivated by vehicular applications where a vehicle (or the infrastructure) equipped with a mono-static radar wishes to communicate data to its target receiver, while estimating parameters of interest related to this receiver. Provided that the radar-equipped transmitter is ready to send data to its target receiver, this setting naturally assumes that the receiver has been already detected. In a point-to-point communication setting over multipath time-frequency selective channels, we study the joint radar and communication system from two perspectives, i.e., the radar parameter estimation at the transmitter as well as the data detection at the receiver. For the radar parameter estimation part, we derive an efficient approximated Maximum Likelihood algorithm and the corresponding Cramér-Rao lower bound for range and velocity estimation. Numerical examples demonstrate that multi-carrier digital formats such as OTFS can achieve as accurate radar estimation as state-of-the-art radar waveforms such as frequency-modulated continuous wave (FMCW). For the data detection part, we focus on separate detection and decoding and consider a soft-output detector that exploits efficiently the channel sparsity in the Doppler-delay domain. We quantify the detector performance in terms of its *pragmatic capacity*, i.e., the achievable rate of the channel induced by the signal constellation and the detector soft-output. Simulations show that the proposed scheme outperforms concurrent state-of-the-art solutions. Overall, our work shows that a suitable digitally modulated waveform enables to efficiently operate joint radar parameter estimation and communication by achieving full information rate of the modulation and near-optimal radar estimation performance. Furthermore, OTFS appears to be particularly suited to the scope.**

***Index Terms*—OTFS, Joint radar parameter estimation and communication, Maximum Likelihood detection, Message-passing, Achievable rate.**

## I. Introduction

A key-enabler of high-mobility networks is the ability of a node to continuously track its dynamically changing environment (state) and react accordingly. Although state sensing and communication have been designed separately in the past, power and spectral efficiency and hardware costs encourage the integration of these two functions, such that they are operated by sharing the same frequency band and hardware (see e.g. [1]). Motivated by emerging vehicular applications (V2X) [2], we consider a *joint radar parameter estimation and communication* system where a radar-equipped transmitter wishes to transmit information to a target receiver and jointly estimate the parameters of that receiver such as range and velocity. It is implicitly assumed that the target has been already detected in an initial acquisition, as radar parameter estimation and communication are jointly performed. This initial target acquisition can be achieved using high resolution radar detection approaches (see [3] and references therein), beam sweeping and beacon-based initial acquisition [4]–[7] as in communication system standards (see [8] and references therein), or a combination thereof.

Such a communication setup has been extensively studied in the literature (see [7], [9]–[17] and references therein). Existing works on joint radar and communications can be roughly classified into two classes. The first class considers some resource-sharing approach, such that time, frequency, or space resources are split into either radar or data communication (e.g., see [12, Section III. A, C] and references therein). The second class uses a common waveform for both radar and communication. This approach includes information-embedded radar waveforms (e.g., see [12, Section III. D], [1, Section IV. A], [15], and references therein) as well as the direct usage of standard communication waveforms applied to radar detection (e.g., see [1, Section IV. B], [1, Section III. B], [9], [11], [18]–[20]). It is worth noticing that a synergistic waveform design for joint radar and communications yields a significant potential gain compared to the resource-sharing approach, as demonstrated in a simplified albeit representative information theoretic framework in [21]. It is also worthwhile to notice that typical V2X channels are characterized by a relatively small number of discrete multipath components corresponding to line-of-sight (LoS) propagation, ground reflection, and some specular reflections on surrounding (e.g., metal) surfaces, each of which is characterized by its own, possibly large, Doppler frequency shift (e.g., see [22], [23] and references therein). Motivated by this fact, we focus on a joint radar and communication system using orthogonal time frequency space (OTFS) modulation (see [24], [25] and references therein), as this modulation format provides inherent robustness to Doppler shifts and is naturally suited to sparse channels in the delay-Doppler domain [26], [27].

The first part of this paper focuses on the suitability of OTFS for joint radar parameter estimation and data communication, by considering the mean square error (MSE) of range and velocity estimation and the achievable rate with Gaussian inputs for a simple point-to-point communication scenario. We extend our preliminary work [28], which considered only

L. Gaudio and G. Colavolpe are with the Department of Engineering and Architecture, University of Parma, Parma, Italy (emails: lorenzo.gaudio@studenti.unipr.it, giulio.colavolpe@unipr.it).

Mari Kobayashi is with the Technical University of Munich, Munich, Germany (email: mari.kobayashi@tum.de).

Giuseppe Caire is with the Department of Electrical Engineering and Computer Science, Technical University of Berlin, 10623 Berlin, Germany (email: caire@tu-berlin.de).

LoS propagation, to the case of a channel with multiple paths, one of which is the LoS, while the other multipath components correspond to unwanted reflections or "clutters", such that the antenna sidelobes are fully taken into account in our signal model (detailed in Section II). We propose an efficient approximated Maximum Likelihood (ML) algorithm to estimate the range and velocity of the target from the backscattered signal and derive the corresponding Cramér-Rao lower bound (CRLB). Our numerical examples inspired by the parameters of IEEE 802.11p demonstrate that digital multi-carrier modulation formats such as OTFS and orthogonal frequency division multiplexing (OFDM) yield as accurate estimation performance as frequency modulated continuous wave (FMCW), one of the typical automotive radar waveforms [10], while achieving significant communication rates. These results suggest that joint radar parameter estimation and communication can be effectively operated without compromising neither the achievable data rates nor the radar performance.

The second part of the paper addresses more specifically the soft-output symbol detection for OTFS at the receiver side. We consider separate detection and decoding and evaluate several options for soft-output symbol detection in terms of their *pragmatic capacity*, i.e., the achievable rate of the channel induced by the signal constellation used with uniform probability at the input and the detector soft output [29], [30]. This performance metric characterizes information theoretical rates achievable by separate detection and decoding, when a specific signal constellation and a specific soft-output symbol detector are employed. Therefore, it is more meaningful and practically relevant than uncoded bit error rate, as usually considered in concurrent works. We propose a message-passing (MP) detector derived from the general approach of [31], suitably adapted to the OTFS signal format. The proposed scheme is compared with the following approaches: i) another MP-based scheme recently proposed in [25]; ii) the standard linear minimum mean square error (MMSE) block equalizer, which is prohibitively complex due to its computation of a large-dimensional matrix inversion; iii) a recently proposed low-complexity approximated linear MMSE equalizer [32], based on some drastic simplifying assumptions that provide a conveniently structured channel matrix for which the large dimensional matrix inversion can be avoided. Our simulation results show that the proposed detection scheme significantly outperforms all other low-complexity schemes, and it is also able to outperform the high-complexity MMSE block equalizer when the channel is sufficiently sparse.

The main contributions of this work are summarized as follows:

1) we propose an efficient algorithm to estimate range and velocity for OTFS modulation employing practical rectangular pulses over a $P$-path time-frequency selective radar channel. The proposed algorithm is different from the one recently proposed in [20]. While [20] focuses on a low-complexity matched filter approach, we consider ML parameter estimation. Our proposed algorithm coincides with the ML estimator for a single path channel ($P = 1$) and it performs also very well for $P > 1$. Furthermore, our proposed algorithm is able to handle continuous values of delay and Doppler, contrary to [20] that assumes discretized delays.

2) We derive the CRLB of range and velocity estimation for a general $P$-path time-frequency selective channel. For the special case of a single-path channel ($P = 1$), we also analyze the typical transition behavior of the ML estimator (usually referred to as *waterfall*), following an approach similar to [33], [34].

3) Through these analytical results and computer simulations, we show that fully digitally modulated waveforms such as OTFS and OFDM provide as accurate range and velocity estimation as FMCW, one of typical radar waveforms. Furthermore, OTFS achieves slightly better data rates than OFDM since the latter incurs a higher overhead due to the cyclic prefix (CP).

4) We adapt the MP-based detection scheme of [31] to the OTFS format, evaluating its performance in terms of pragmatic capacity. Our scheme improves upon existing works in various aspects. First, we consider OTFS modulation with practical rectangular pulses, rather than ideal pulses satisfying the bi-orthogonal condition as considered in [24], [32], [35]. Unfortunately such ideal pulses are mathematically impossible to construct [36]. Second, our method constructs a *Factor Graph (FG)* (e.g., [37]) of girth 6, for which the exact sum-product algorithm (SPA) (e.g., [37]) can be directly applied with linear complexity in the symbol constellation size, as opposed to the MP detector of [25], based on a FG of girth 4 and requiring a Gaussian approximation of the interfering constellation symbols in order to avoid high complexity computations (more details on this point are discussed in Section V). Finally, our scheme does not make simplifying assumptions on the channel model such as discretized delay and Doppler shifts and/or exactly bi-orthogonal pulses, therefore it is much more robust to realistic system and channel conditions.

The paper is organized as follows. In Section II, we present the physical model. In Section III, we derive the OTFS input-output relation and the definition of the channel matrix. In Section IV, we provide the ML radar estimator together with the theoretical analysis of the ML estimation performance. Section V introduces the considered symbol detection algorithms. In Section VI, we define the chosen performance metrics and then we show some illustrative numerical results. Finally, Section VII concludes the paper.

## II. Physical model

We consider a joint radar parameter estimation and communication system over a channel bandwidth $B$ operating at the carrier frequency $f_c$. We assume that a transmitter, equipped with a mono-static full-duplex radar, wishes to convey a message to its target receiver while estimating parameters of interest related to the same receiver from the backscattered signal. Full-duplex operations can be achieved with sufficient isolation between the transmitter and the (radar) detector and possibly interference analog pre-cancellation in order to prevent the (radar) detector saturation [38]. For simplicity, in this paper we consider no self-interference, keeping in mind that some residual self-interference can be handle as additional noise [18].

We model a generic $P$-taps time-frequency selective channel according to the time-varying impulse response [39]

$$h(t,\tau) = \sum_{p=0}^{P-1} h_p e^{j2\pi\nu_p t}\delta\left(\tau-\tau_p\right)\,, \tag{1}$$

where $P$ denotes the number of scattering reflections or paths and the 0-th path is the LoS, $h_p$ is a complex channel gain including the path loss (PL) of the path component, while $\nu_p = \frac{v_p f_c}{c}$, $\tau_p = \frac{r_p}{c}$, $v_p$, and $r_p$ denote the corresponding one-way Doppler shift, delay, velocity, and range associated to the $p$-th propagation path, respectively, with $c$ denoting the speed of light.

Note that (1) indicates the general form of the channel impulse response, and it is used in Section III to derive the input-output relation of the block-wise complex baseband equivalent channel induced by OTFS. Then, for the sake of simplicity, we shall keep the same notation to indicate both the impulse response of the radar backscattered channel in Section IV and the impulse response of the transmitter to receiver data communication channel in Section V. The same holds for the backscattered radar signal received at the transmitter and the received signal at the communication receiver. Since the two problems are treated separately and in different sections, there is no danger of confusion. Of course, in the case of radar parameter estimation, the complex channel gain of each multipath component $h_p$ takes into account the two-way PL as well as the cross section $\sigma_{\rm rcs}$ of the target causing the reflection, and $\tau_p$ and $\nu_p$ denote the two-way delay and Doppler shifts. Therefore, the time of flight and Doppler shift related to relative range and velocity of the target with respect to the radar transmitter/receiver are obtained by dividing by 2 the estimated parameters $\tau_0$ and $\nu_0$ corresponding to the shortest path, which corresponds to the LoS reflection and which is assumed to exist in the radar problem setting. Considering a generic antenna gain $G$, we define the radar and communication SNRs as [40, Chapter 2]

$$\mathrm{SNR}_{\rm rad} = \frac{\lambda^2\sigma_{\rm rcs}G^2}{(4\pi)^3 r^4}\frac{P_{\rm avg}}{\sigma_w^2}\,,\ \mathrm{SNR}_{\rm com} = \frac{\lambda^2 G^2}{(4\pi)^2 r^2}\frac{P_{\rm avg}}{\sigma_w^2}\,, \tag{2}$$

respectively, where $\lambda = c/f_c$ is the wavelength, $\sigma_{\rm rcs}$ is the radar cross-section in $\mathrm{m}^2$, and $r$ is the distance between transmitter and receiver in the communication case or between transmitter and target in the radar case.

We assume that the transmitter periodically scans narrow angular sectors (e.g., using a phased array). If the sector beam is narrow enough, it is reasonable to consider a single target in each sector, while the propagation can go through multiple paths, one of which is the LoS, and the others may be caused by ground reflection, reflections on buildings and metal surfaces (e.g., vehicles parked along the street), and other unwanted echoes or clutters (also from the sidelobes of the antenna beamforming pattern). For these reasons, our model is fully general and is able to handle most of the impairments of an automotive scenario (or any other scenario including scattering components and moving equipment). An example of this scenario is depicted in Fig. 1. Note that the presence of the target in the scanned angular sector is given for granted, since an initial target detection/acquisition phase (with related false alarm and miss detection probabilities) is performed before the joint radar parameter estimation and communication phase. We thus focus on the estimation of the delay (related to the range between transmitter and receiver) and of the Doppler shift (related to the relative velocity between transmitter and receiver) of the LoS path, since in the envisaged scenario the direction of arrival is automatically determined by the scanned angular sector.

Due to the aforementioned reasons, our work neglects some typical problems related to radar target detection. For instance, within the transmitted beam, there could be a target with a "small" radar cross section in front of some "bigger" target with larger cross section in the background. If the separation of the two targets in the Doppler-delay plane is below the Doppler and delay resolution of the radar system, the two targets are indistinguishable and the larger target masks the smaller one. In this case radar is not able to detect the presence of the smaller target. This problem is inherent to the resolvability of multiple targets in the Doppler-delay grid, whose resolution depends on the time duration and signal bandwidth of the transmitted waveform, which in our case coincides with an OTFS data block. On the other hand, if multiple targets are sufficiently well separated in the Doppler-delay plane, the algorithm proposed in this paper can be extended to estimate the radar parameters of multiple targets through a threshold-based approach rather than just look at maximization of the likelihood function as described Section IV. In the follow-up work [41] we explicitly treat the detection/acquisition of multiple targets with multiple-input multiple-output (MIMO) OTFS, i.e., considering also the additional angle dimension, as an extension of the approach presented in this paper.

## III. OTFS Input-Output Relation

We derive here the input-output discrete complex baseband model for the OTFS signal format by generalizing previous works [24], [25], removing certain oversimplifying assumptions such as bi-orthogonal pulses and discretized delay and/or Doppler shifts.

As usually done in OTFS modulation (e.g., [24], [25]), data symbols $\{x_{k,l}\}$, for $k = 0,\dots,N-1$ and $l = 0,\dots,M-1$, are arranged in an $N \times M$ two-dimensional grid referred to as the Doppler-delay domain. We consider the average power constraint given by

$$\frac{1}{NM}\sum_{k=0}^{N-1}\sum_{l=0}^{M-1}\mathbb{E}\left[\left|x_{k,l}\right|^2\right] \le P_{\rm avg}\,. \tag{3}$$

In order to send the block of symbols $\{x_{k,l}\}$, the transmitter first applies the inverse symplectic finite Fourier transform (ISFFT) to convert data symbols into a block of samples $\{X[n,m]\}$ in the dual domain, referred to as the time-frequency domain. This is given by

$$X\left[n,m\right] = \sum_{k=0}^{N-1}\sum_{l=0}^{M-1} x_{k,l}e^{j2\pi\left(\frac{nk}{N}-\frac{ml}{M}\right)}, \tag{4}$$

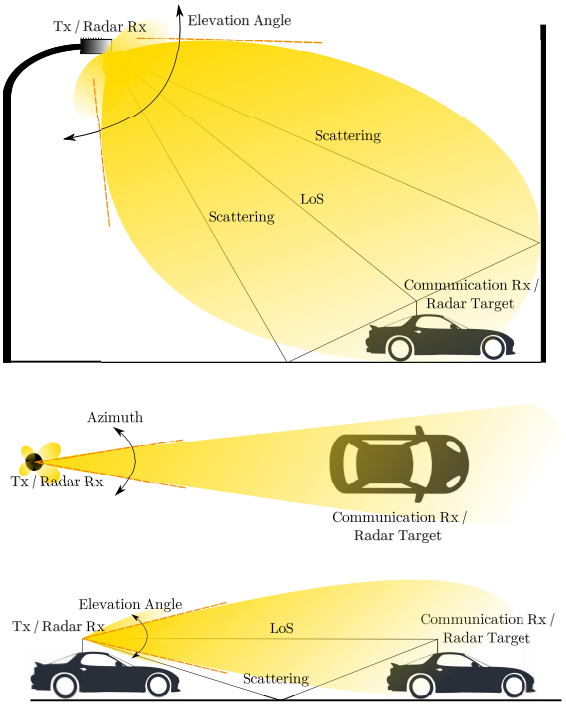


Fig. 1. The figure shows the beam sweeping scenario of our work. Between the transmitter (Tx) and the radar target there is a LoS component and some scattering paths, depending on the surrounding environment. The Rx (e.g., a car in this case) "passively" reflects the incoming signal back to the Radar Rx (co-located with the Tx).

for $n = 0, \dots, N-1$ and $m = 0, \dots, M-1$. Then, it generates the continuous-time signal

$$s(t) = \sum_{n=0}^{N-1} \sum_{m=0}^{M-1} X[n,m]\, g_{\text{tx}}(t - nT)\, e^{j2\pi m \Delta f (t-nT)}, \quad (5)$$

where $g_{\text{tx}}(t)$ denotes the transmit shaping pulse, $T$ is the symbol duration, and we consider a multi-carrier system where the total bandwidth is divided into $M$ subcarriers, i.e., $B = M\Delta f$, where $\Delta f = 1/T$ denotes the subcarrier spacing. By considering $g_{\text{tx}}(t)$ strictly time limited in $[0, T]$, the OTFS frame duration is given by $T_f^{\text{otfs}} = NT$ (generally the duration is larger, but in practice it is well approximated by $NT$ up to some guard interval containing the "tail" of $g_{\text{tx}}(t)$). The noiseless received signal $r(t)$ after transmission through the time-frequency selective channel in (1) is given by

$$r(t) = \int h(t,\tau) s(t-\tau) d\tau = \sum_{p=0}^{P-1} h_p s(t-\tau_p) e^{j2\pi\nu_p t}, \quad (6)$$

while the output of the receiver filter-bank adopting a generic receive shaping pulse $g_{\text{rx}}(t)$ is

$$Y(t,f) = \int r(t')\, g_{\text{rx}}^*(t'-t)\, e^{-j2\pi f t'} dt'. \quad (7)$$

By sampling at $t = nT$ and $f = m\Delta f$, the received samples in the time-frequency domain are given by

$$\begin{aligned} Y[n,m] &= Y(t,f)|_{t=nT, f=m\Delta f} \\ &= \sum_{n'=0}^{N-1} \sum_{m'=0}^{M-1} X[n',m']\, H_{n,m}[n',m'], \end{aligned} \quad (8)$$

where, by letting $h'_p \triangleq h_p e^{j2\pi\nu_p\tau_p}$, we have

$$\begin{aligned} H_{n,m}[n',m'] &\triangleq \sum_{p=0}^{P-1} h'_p e^{j2\pi n' T \nu_p} e^{-j2\pi m \Delta f \tau_p} \\ &\times C_{g_{\text{tx}},g_{\text{rx}}}((n-n')T - \tau_p, (m-m')\Delta f - \nu_p), \end{aligned} \quad (9)$$

where $C_{u,v}(\tau,\nu) \triangleq \int_{-\infty}^{\infty} u(t)\, v^*(t-\tau)\, e^{-j2\pi\nu t} dt$ denotes the cross-ambiguity function between two generic pulses $u$ and $v$, as defined in [36]. Finally, the received samples in the Doppler-delay domain are obtained by applying the symplectic finite Fourier transform (SFFT) to (8), i.e.,

$$\begin{aligned} y[k,l] &= \frac{1}{NM} \sum_{n=0}^{N-1} \sum_{m=0}^{M-1} Y[n,m]\, e^{-j2\pi\left(\frac{nk}{N} - \frac{ml}{M}\right)} \\ &= \sum_{k'=0}^{N-1} \sum_{l'=0}^{M-1} x_{k',l'} g_{k,k'}[l,l'], \end{aligned} \quad (10)$$

where the inter-symbol interference (ISI) coefficient of the Doppler-delay pair $[k',l']$ seen by sample $[k,l]$ is given by

$$g_{k,k'}[l,l'] = \sum_{p=0}^{P-1} h'_p \boldsymbol{\Psi}^p_{k,k'}[l,l'], \quad (11)$$

where the channel matrix entries $\boldsymbol{\Psi}^p_{k,k'}[l,l']$ are defined in (12). Writing the $N \times M$ matrices of transmitted symbols and received samples as $NM$-dimensional column vectors (stacking the columns of the corresponding matrices on top of each other), we obtain the block-wise input-output relation as

$$\boldsymbol{y} = \underbrace{\left(\sum_{p=0}^{P-1} h'_p \boldsymbol{\Psi}_p\right)}_{\boldsymbol{\Psi}} \boldsymbol{x} + \boldsymbol{w}, \quad (13)$$

where $\boldsymbol{\Psi}_p$ is the $NM \times NM$ matrix obtained from (12) while $\boldsymbol{w}$ denotes the additive white Gaussian noise (AWGN) with zero mean and covariance $\sigma_w^2 \mathbf{I}_{NM}$. Notice that our input-output relation in (13) is exact (i.e., no approximation was made in its derivation) and holds for any pair of transmit/receive pulses.

In order to proceed further in a tractable manner, as done in [25], we approximate the integral of the cross-ambiguity function with a discrete sum. In particular, we write

$$\begin{aligned} C_{g_{\text{rx}},g_{\text{tx}}}(\tau,\nu) &= \int_0^T g_{\text{tx}}(t)\, g_{\text{rx}}^*(t-\tau)\, e^{-j2\pi\nu t} dt \\ &\approx \frac{T}{M} \sum_{i=0}^{M-1} g_{\text{tx}}\left(i\frac{T}{M}\right) g_{\text{rx}}^*\left(i\frac{T}{M} - \tau\right) e^{-j2\pi\nu i \frac{T}{M}}, \end{aligned} \quad (14)$$

where, for analytical convenience, the number of equally spaced discretization nodes is equal to the number of subcarriers $M$. This approximation is accurate provided that $M$ is large enough, which is the typical case. Now, by letting $g_{\text{tx}}(t)$ and $g_{\text{rx}}(t)$ be rectangular pulses of length $T$, by limiting the channel delay to $\tau_{\max} < T$, it readily follows that the cross-ambiguity function yields non-zero samples only for $n' = n$ and $n' = n-1$. Hence, the entries of the cross-talk matrix $\boldsymbol{\Psi}^p_{k,k'}[l,l']$ can be written as in (15), in which we exploited

$$\boldsymbol{\Psi}_{k,k'}^{p}\left[l,l'\right]=\sum_{n,n',m,m'}e^{j2\pi n'T\nu_p}e^{-j2\pi m\Delta f\tau_p}e^{-j2\pi\left(\frac{nk}{N}-\frac{ml}{M}-\frac{n'k'}{N}+\frac{m'l'}{M}\right)}\frac{C_{g_{\mathrm{rx}},g_{\mathrm{tx}}}\left(\left(n-n'\right)T-\tau_p,\left(m-m'\right)\Delta f+\nu_p\right)}{NM} \tag{12}$$

$$\boldsymbol{\Psi}_{k,k'}^{p}\left[l,l'\right]\approx\frac{1}{NM}\frac{1-e^{j2\pi\left(k'-k+\nu_pNT\right)}}{1-e^{j2\pi\frac{\left(k'-k+\nu_pNT\right)}{N}}}\frac{1-e^{j2\pi\left(l'-l+\tau_pM\Delta f\right)}}{1-e^{j2\pi\frac{\left(l'-l+\tau_pM\Delta f\right)}{M}}}e^{-j2\pi\nu_p\frac{l'}{M\Delta f}}\begin{cases}1 & \text{if } l'\in\mathcal{L}_{\mathrm{ICI}}\\ e^{-j2\pi\left(\frac{k'}{N}+\nu_pT\right)} & \text{if } l'\in\mathcal{L}_{\mathrm{ISI}}\end{cases} \tag{15}$$

the expression of the approximated cross-ambiguity function for rectangular pulses given by

$$C_{g_{\mathrm{rx}},g_{\mathrm{tx}}}\left(\tau,\nu\right)\approx\frac{1}{M}\sum_{i=0}^{M-1-l_\tau}\exp\left(-j2\pi\nu i\frac{T}{M}\right), \tag{16}$$

with $l_\tau\triangleq\lceil\tau/\left(T/M\right)\rceil$, and where we defined the index sets

$$\begin{cases}\mathcal{L}_{\mathrm{ICI}}\triangleq\left[0,M-1-l_{\tau_p}\right]\\ \mathcal{L}_{\mathrm{ISI}}\triangleq\left[M-l_{\tau_p},M-1\right]\end{cases}. \tag{17}$$

The details of the derivation are highlighted in the Appendix.

Moreover, in order to have the received signal bandwidth still approximately equal to $B$, we must assume that the bandwidth expansion due to Doppler is negligible with respect to $B$. In our case, for the sake of simplicity, we make the usual assumption that $\nu_{\max}<\Delta f$.[1]

## IV. OTFS Radar Parameter Estimation

### A. Maximum Likelihood Estimator

Focusing on the channel model defined in (1) with a single target and multiple backscattered paths, we wish to find the ML estimator for the set of $3P$ unknown parameters $\bar{\boldsymbol{\theta}}=\left(\bar{h}'_0,\ldots,\bar{h}'_{P-1},\bar{\tau}_0,\ldots,\bar{\tau}_{P-1},\bar{\nu}_0,\ldots,\bar{\nu}_{P-1}\right)$, where the bar indicates the true value of the unknown parameters.

By using expression (15) for the channel matrix coefficients, which contains the dependency on the parameters $\{\tau_p,\nu_p\}$, the log-likelihood function to be minimized is given by

$$l\left(\boldsymbol{y}|\boldsymbol{\theta},\boldsymbol{x}\right)=\left\|\boldsymbol{y}-\sum_{p=0}^{P-1}h'_p\boldsymbol{\Psi}_p\boldsymbol{x}\right\|^2, \tag{18}$$

where symbols in $\boldsymbol{x}$ are known at the radar detector, since it is co-located with the transmitter. Therefore, these symbols are treated as known (in the conditioning), and not as nuisance as for classical timing and frequency estimators, and the receiver performs coherent processing. The ML estimator is given by

$$\hat{\boldsymbol{\theta}}=\arg\min_{\boldsymbol{\theta}\in\mathbb{C}^P\times\mathbb{R}^P\times\mathbb{R}^P}l\left(\boldsymbol{y}|\boldsymbol{\theta},\boldsymbol{x}\right). \tag{19}$$

A brute-force search for the maximum in a $3P$-dimensional continuous domain is unfeasible in general. Thus, in the following we propose a viable method to approximate the ML solution with low complexity.

[1]Note that this approximation can be justified in a number of scenarios. For example, consider a scenario inspired by IEEE 802.11p with $f_c=5.89$ GHz and the subcarrier spacing $\Delta f=156.25$ KHz. This yields $v_{\max}<14325$ km/h, which is reasonable even for a relative speed of 400 km/h. The same holds for IEEE 802.11ad with $f_c$ = 60 GHz and $\Delta f=5.15625$ MHz [42].

The log-likelihood function in (18) is quadratic in the complex amplitudes $\{h'_p\}$ for given $\{\tau_p,\nu_p\}$. Hence, the minimization of (18) w.r.t. $\{h'_p\}$ for fixed $\{\tau_p,\nu_p\}$ is readily given as the solution of the linear system of equations

$$\sum_{q=0}^{P-1}h'_q\boldsymbol{x}^H\boldsymbol{\Psi}_p^H\boldsymbol{\Psi}_q\boldsymbol{x}=\boldsymbol{x}^H\boldsymbol{\Psi}_p^H\boldsymbol{y},\quad p=0,\ldots,P-1. \tag{20}$$

Expanding (18) and using the equality (20), after some long but relatively simple algebra (not given explicitly for the sake of brevity), we find that the minimization with respect to $\{\tau_p,\nu_p\}$ reduces to maximizing the function

$$l_2(\boldsymbol{y}|\boldsymbol{\theta},\boldsymbol{x})=\sum_{p=0}^{P-1}\Bigg\{\overbrace{\frac{|\boldsymbol{x}^H\boldsymbol{\Psi}_p^H\boldsymbol{y}|^2}{\boldsymbol{x}^H\boldsymbol{\Psi}_p^H\boldsymbol{\Psi}_p\boldsymbol{x}}}^{S_p(\tau_p,\nu_p)}\underbrace{-\frac{\left(\sum_{q\neq p}h'_q\boldsymbol{x}^H\boldsymbol{\Psi}_p^H\boldsymbol{\Psi}_q\boldsymbol{x}\right)\boldsymbol{y}^H\boldsymbol{\Psi}_p\boldsymbol{x}}{\boldsymbol{x}^H\boldsymbol{\Psi}_p^H\boldsymbol{\Psi}_p\boldsymbol{x}}}_{I_p\left(\{h'_q\}_{q\neq p},\boldsymbol{\tau},\boldsymbol{\nu}\right)}\Bigg\}, \tag{21}$$

where $S_p$ and $I_p$ denote the useful signal and the interference for path $p$, respectively. Clearly, since the channel coefficients $\{h'_p\}$ are not known, it is impossible to directly maximize $l_2\left(\boldsymbol{y}|\boldsymbol{\theta},\boldsymbol{x}\right)$ w.r.t. $\{\tau_p,\nu_p\}$. Furthermore, even for known coefficients $\{h'_p\}$, the function $l_2\left(\boldsymbol{y}|\boldsymbol{\theta},\boldsymbol{x}\right)$ is not separable in the pairs of parameters $(\tau_p,\nu_p)$ for different values of $p$ because of the dependency of the interference terms $I_p$ on all $(\tau_q,\nu_q)$ for $q\neq p$. Nevertheless, this dependency appears through the "cross-term" coefficients of the type $\boldsymbol{x}^H\boldsymbol{\Psi}_p^H\boldsymbol{\Psi}_q\boldsymbol{x}$, which tend to be weak for typically sparse multipath channels. Therefore, we resort to an iterative block-wise optimization that alternates the optimization of each pair $(\tau_p,\nu_p)$ by keeping fixed the other parameter pairs and the channel complex coefficients and, after a round of updates for the delay and Doppler parameters, it re-evaluates the estimates of the channel coefficients by solving (20). The algorithm steps are given in the following, where the iteration index is denoted in brackets by $n^{\mathrm{it}}$:

1) *Initialization:* let $n^{\mathrm{it}}=0$ and $\hat{h}'_p[0]=0$ for all $p=0,\ldots,P-1$.
2) For $n^{\mathrm{it}}=1,2,3,\ldots$ repeat:
   - Delay and Doppler shift update: for each $p=0,\ldots,P-1$, find the estimates $\hat{\tau}_p[n^{\mathrm{it}}],\hat{\nu}_p[n^{\mathrm{it}}]$ by

solving the two-dimensional maximization

$$\left(\hat{\tau}_p[n^{\mathrm{it}}], \hat{\nu}_p[n^{\mathrm{it}}]\right) = \arg \max_{(\tau_p, \nu_p)} \Big\{ S_p\left(\tau_p, \nu_p\right) - I_p\left(\{\hat{h}'_q\}_{q \neq p}, \tau_p, \nu_p, \{\hat{\tau}_q, \hat{\nu}_q\}_{q \neq p}\right) \Big\}, \quad (22)$$

where $\hat{\tau}_q$, $\hat{\tau}_q$, and $\hat{\nu}_q$ belong to $\left[n^{\mathrm{it}} - 1\right]$.

- Complex channel coefficients update: solve the linear system (20) for the channel matrices $\{\boldsymbol{\Psi}_p\}$ calculated with parameters $\{\hat{\tau}_p[n^{\mathrm{it}}], \hat{\nu}_p[n^{\mathrm{it}}]\}$, and let the solution be denoted by $\{\hat{h}'_p[n^{\mathrm{it}}]\}$.

The iteration stops when the values of $\{\hat{\tau}_p[n^{\mathrm{it}}], \hat{\nu}_p[n^{\mathrm{it}}]\}$ do not show a significant change with respect to the previous iteration, or if a maximum number of iterations is reached. In practice, we find the maximizer in (22) first by searching on the "integer" Doppler-delay grid, for which the channel matrices have been pre-calculated and stored, then by searching on a finely discretized grid $\Gamma$ on the delay and Doppler domains, around the rough estimated value of the first phase. This two (or even multiple) step maximization search allows to reduce the overall computational complexity, allowing to adopt the proposed algorithm even with increasing block dimensions $NM$ (up to a certain limit). Furthermore, in all our simulations we noticed that the algorithm converges in just a few iterations (2 to 5, at most). Note that the case $P = 1$, which corresponds to the presence of the term $S_0(\tau_0, \nu_0)$ only with no interfering terms $I_p$, is simply the adaptive matched filter introduced in [43].

### B. Performance Bounds

*1) Cramér-Rao lower bound (CRLB):* The derivation of the CRLB is based on the channel matrix expression in (15). From the channel model (1), by letting

$$s_p[k,l] = \left|h'_p\right| e^{j \angle h'_p} \sum_{k'=0}^{N-1} \sum_{l'=0}^{M-1} \boldsymbol{\Psi}^p_{k,k'}\left[l, l'\right] x_{k',l}\,, \quad (23)$$

and considering separately the amplitude and the phase of the complex channel coefficients $\{h'_p\}$, the $(i,j)$ element of the $4P \times 4P$ Fisher information matrix is given by

$$\left[\mathbf{I}(\boldsymbol{\theta}, \boldsymbol{x})\right]_{i,j} = \frac{2P_{\mathrm{avg}}}{\sigma_w^2} \mathrm{Re}\left\{ \sum_{n,m} \left[\frac{\partial s_p[n,m]}{\partial \theta_i}\right]^* \frac{\partial s_p[n,m]}{\partial \theta_j} \right\}, \quad (24)$$

in which $\boldsymbol{\theta} = \left(\left|\boldsymbol{h}'\right|, \angle \boldsymbol{h}', \boldsymbol{\tau}, \boldsymbol{\nu}\right)$ is the set of $4P$ channel unknown parameters.

The partial derivatives w.r.t. the magnitude and phase of $h'_p$ are straightforward and are omitted for the sake of space limitation. The derivatives w.r.t. $\tau_p$ and w.r.t. $\nu_p$ are more cumbersome and, after some algebra, can be obtained in expressions (25) and (26), respectively. The desired CRLB follows by filling the Fisher information matrix in (24) with the derivatives computed above, and obtaining the diagonal elements of the inverse Fisher information matrix. In particular, we are interested in the CRLB for the parameters $\tau_0$ and $\nu_0$, related to the target range and velocity.

*2) Waterfall Analysis for $P = 1$:* In the case of $P = 1$ our iterative scheme reduces to the exact joint ML estimation of $h'_0, \tau_0, \nu_0$ (in other words, the iterative scheme converges after the first iteration to the exact maximum of the log-likelihood function, up to the discretization error in the 2-dimensional search domain $\Gamma$). It is well-known that ML estimators typically exhibit a threshold effect, i.e., a rapid deterioration of the estimation MSE when the signal-to-noise ratio (SNR) is below some threshold (that generally depends on the problem and on the sample size). In contrast, for SNR larger than such threshold the ML estimator yields MSE typically very close to the CRLB. This waterfall behavior is caused by "outliers" in the search of the maximum in ML estimator: namely, when the observation is too noisy, the maxima of the likelihood functions tend to be randomly placed anywhere on the search grid. In the following we provide an analysis of the waterfall transition for the case $P = 1$, i.e., the region around the threshold SNR value where the rapid deterioration occurs. Our simulations show that the waterfall prediction provided by our analysis for $P = 1$ is also very accurate for the multipath case $P > 1$. This corroborates the evidence that our proposed approximated ML algorithm is effectively very good, and performs very close to the true ML.[2]

Following the reasoning of [33], [34], we treat as "outlier" the event that a maximum of the log-likelihood function is randomly placed on the grid $\Gamma$, rather than in the cluster of points around the true value $(\bar{\tau}_0, \bar{\nu}_0)$. Let $\alpha \in \{\tau, \nu\}$ be the unknown parameter to be estimated. By the law of total probability over the discretized grid $\Gamma$ (where we calculate the ML estimator), we can express the estimation MSE as

$$\begin{aligned} \mathrm{MSE} = E\left[\left(\hat{\alpha} - \bar{\alpha}\right)^2\right] &= \sum_{i \in \Gamma} \Pr\left(\epsilon\left(i\right)\right) \left(\hat{\alpha}_i - \bar{\alpha}\right)^2 \\ &\leq \sum_{i \in \Gamma} \Pr\left(\tilde{\epsilon}\left(i\right)\right) \left(\hat{\alpha}_i - \bar{\alpha}\right)^2 . \end{aligned} \quad (27)$$

where $\bar{\alpha}$ is the true value of the parameter, $\hat{\alpha}$ is the estimated parameter, and $\Pr\left(\epsilon\left(i\right)\right)$ denotes the probability of error of choosing $\alpha_i$ rather than $\bar{\alpha}$. While evaluating $\Pr\left(\epsilon\left(i\right)\right)$ may be extremely difficult, we obtain an upper bound by considering pairwise error probabilities, i.e., replacing $\Pr\left(\epsilon\left(i\right)\right)$ with the probability that the detector chooses $\alpha_i$ rather than $\bar{\alpha}$ when these are the only two alternatives. Since the pairwise error event $\tilde{\epsilon}\left(i\right)$ contains the true error event $\epsilon(i)$, it follows that the inequality of (27) provides an upper bound.

Proceeding further, we define the pairwise error probability as

$$\Pr\left(\tilde{\epsilon}\left(i\right)\right) \triangleq \Pr\left\{ l\left(\boldsymbol{y}|\boldsymbol{\theta}_i, \boldsymbol{x}\right) < l\left(\boldsymbol{y}|\bar{\boldsymbol{\theta}}, \boldsymbol{x}\right) \right\}, \quad (28)$$

where $l\left(\boldsymbol{y}|\boldsymbol{\theta}_i, \boldsymbol{x}\right)$ and $l\left(\boldsymbol{y}|\bar{\boldsymbol{\theta}}, \boldsymbol{x}\right)$ are the values obtained from the evaluation of the likelihood function at grid points $i$ with parameters $\boldsymbol{\theta}_i$ and using the true parameters $\bar{\boldsymbol{\theta}}$, respectively. At this point, the problem is reduced to the computation of the

[2]Obviously, the CRLB for $P = 1$ yields also a lower bound for the case $P > 1$, in the case where we simply add more multipath components on top of the LoS component without changing the statistics of the LoS component, since the presence of more unknown parameters cannot help the estimation of the target parameters $\tau_0, \nu_0$.

$$\frac{\partial \boldsymbol{\Psi}_{k,k'}\left[l,l'\right]}{\partial \tau_p} = \sum_{n,m} e^{j2\pi\left(\nu_p NT-k+k'\right)\frac{n}{N}} e^{j2\pi\left(l-l'-\tau_p M\Delta f\right)\frac{m}{M}} \left(j2\pi m\Delta f\right) \frac{e^{j2\pi\nu_p\left(\frac{l'}{M\Delta f}\right)}}{NM} \begin{cases} 1 & \text{if } l' \in \mathcal{L}_{\text{ICI}} \\ e^{-j2\pi\left(\frac{k'}{N}+\nu_p T\right)} & \text{if } l' \in \mathcal{L}_{\text{ISI}} \end{cases} \tag{25}$$

$$\begin{aligned} \frac{\partial \boldsymbol{\Psi}_{k,k'}\left[l,l'\right]}{\partial \nu_p} &= \frac{j2\pi}{NM} \sum_{m} e^{j2\pi\left(l-l'-\tau_p M\Delta f\right)\frac{m}{M}} e^{j2\pi\nu_p\left(\frac{l'}{M\Delta f}\right)} \\ &\times \begin{cases} \sum_n e^{j2\pi\left(\nu_p NT-k+k'\right)\frac{n}{N}} \frac{l'}{M\Delta f} + \sum_n nTe^{j2\pi\left(\nu_p NT-k+k'\right)\frac{n}{N}} & \text{if } l' \in \mathcal{L}_{\text{ICI}} \\ e^{-j2\pi\left(\frac{k'}{N}+\nu_p T\right)} \left[\sum_n e^{j2\pi\left(\nu_p NT-k+k'\right)\frac{n}{N}} \left(\frac{l'}{M\Delta f} - T\right) + \sum_n nTe^{j2\pi\left(\nu_p NT-k+k'\right)\frac{n}{N}}\right] & \text{if } l' \in \mathcal{L}_{\text{ISI}} \end{cases} \end{aligned} \tag{26}$$

pairwise error probabilities $\Pr\left(\epsilon\left(i\right)\right)$, for $i \in \mathit{\Gamma}$, which can be derived as follows. We notice that

$$\Pr\left(\tilde{\epsilon}\left(i\right)\right) \approx \Pr\left\{|\boldsymbol{x}^H\boldsymbol{\Psi}_i^H\boldsymbol{y}|^2 > |\boldsymbol{x}^H\bar{\boldsymbol{\Psi}}^H\boldsymbol{y}|^2\right\}, \tag{29}$$

where $\bar{\boldsymbol{\Psi}}$ is the channel matrix calculated with the true parameters and we exploit $\boldsymbol{\Psi}_i^H\boldsymbol{\Psi}_i{=}\boldsymbol{I}$, $\forall i$, for $P = 1$. Defining the jointly conditionally Gaussian random variables

$$z_i \triangleq \boldsymbol{x}^H\boldsymbol{\Psi}_i^H\boldsymbol{y} = \boldsymbol{x}^H\boldsymbol{\Psi}_i^H\bar{\boldsymbol{\Psi}}\boldsymbol{x} + \boldsymbol{x}^H\boldsymbol{\Psi}_i^H\boldsymbol{w}, \tag{30}$$

$$\bar{z} \triangleq \boldsymbol{x}^H\bar{\boldsymbol{\Psi}}^H\boldsymbol{y}{=}\boldsymbol{x}^H\boldsymbol{x} + \boldsymbol{x}^H\bar{\boldsymbol{\Psi}}^H\boldsymbol{w}, \tag{31}$$

with first and second order moments

$$\begin{cases} \mathrm{E}\left[\bar{z}\right] = \|\boldsymbol{x}\|^2, & \mathrm{Var}\left[\bar{z}\right] = \sigma_w^2\|\boldsymbol{x}\|^2 \\ \mathrm{E}\left[z_i\right] = \boldsymbol{x}^H\boldsymbol{\Psi}_i^H\bar{\boldsymbol{\Psi}}\boldsymbol{x}, & \mathrm{Var}\left[z_i\right] = \sigma_w^2\|\boldsymbol{x}\|^2 \end{cases}, \tag{32}$$

and

$$\mathrm{Cov}\left[\bar{z}, z_i\right] = \sigma_w^2\boldsymbol{x}^H\bar{\boldsymbol{\Psi}}^H\boldsymbol{\Psi}_i\boldsymbol{x}, \tag{33}$$

a good approximation for $\Pr\left(\tilde{\epsilon}\left(i\right)\right)$ is given by [33]

$$\Pr\left(\tilde{\epsilon}\left(i\right)\right) \approx \frac{1}{2}\exp\left\{\frac{-\|\boldsymbol{x}\|^4}{2\sigma_w^2 NM}\right\} \mathrm{I}_0\left(\frac{\left|\boldsymbol{x}^H\boldsymbol{\Psi}_i^H\bar{\boldsymbol{\Psi}}\boldsymbol{x}\right| \cdot \|\boldsymbol{x}\|^2}{2\sigma_w^2 NM}\right), \tag{34}$$

where $\mathrm{I}_0$ is the modified Bessel function of the first kind of order 0. The MSE estimation can be thus computed by substituting (34) into (27), using the above definitions.

The resulting (approximated) upper bound tends to be loose at low SNR, but becomes more accurate moving towards the ML waterfall region. Furthermore, the MSE strictly depends on the grid resolution and may or may not reach the CRLB for increasing SNR depending on the systematic error incurred by the grid discretization. As a matter of fact, in our numerical results we took care of using a search grid fine enough such that the discretization systematic error is not visible in the explored range of SNR.

In order to cope with the fact that the (approximated) MSE upper bound obtained in (27) becomes very loose for low SNR, we use also the trivial upper bound

$$\mathrm{MSE} \leq \frac{1}{|\mathit{\Gamma}|}\sum_{i\in\mathit{\Gamma}}(\hat{\alpha}_i - \bar{\alpha})^2, \tag{35}$$

that corresponds to choosing at random grid points, by disregarding completely the received signal.

Then, putting together (27) (with the pairwise error probability approximation in (34) and the above "random estimation" bound in (35), we finally obtain the approximated MSE upper bound

$$\mathrm{MSE} \lesssim \min\left\{\sum_{i\in\mathit{\Gamma}} \Pr\left(\tilde{\epsilon}\left(i\right)\right)\left(\hat{\alpha}_i - \bar{\alpha}\right)^2, \sum_{i\in\mathit{\Gamma}} \frac{(\hat{\alpha}_i - \bar{\alpha})^2}{|\mathit{\Gamma}|}\right\}. \tag{36}$$

Our simulations show that this approximated upper bound is very accurate and it is able to predict very well the waterfall behavior of the ML estimator (as well as the proposed approximated ML estimator in the case $P > 1$).

## V. OTFS Soft-Output Data Detection

We will now focus on the OTFS data detection at the receiver side. By considering the communication channel model in (1), in line with most of the current literature on OTFS detection (e.g., [24], [25]) we assume perfect channel state information (CSI) at the receiver. An efficient pilot-aided CSI acquisition is a problem of independent interest that we postpone to future work (see also [26], [27], [44]).

In this paper, we consider separate detection and decoding, where the receiver consists of the concatenation of a soft-output symbol detector, producing soft-estimates of the coded symbols $\boldsymbol{x}$, and a decoder that takes such estimates as the output of a virtual channel that incorporates also the detector. Motivated by practical complexity considerations, no "turbo equalization" involving a feedback loop from the (soft-output) decoder to the detector and iterations between detector and decoder is considered. It follows that the relevant performance measure is the already mentioned pragmatic capacity, i.e., the mutual information between the input constellation symbols, used with uniform probability, and the corresponding detector soft-output [29], [30].

We propose an efficient low-complexity MP-based soft-output detector, obtained by constructing a FG for the joint posterior probability of $\boldsymbol{x}$ given $\boldsymbol{y}$ in (13) and applying the standard SPA computation rules to compute its marginals. The FG is constructed according to the general approach of [31] (applicable to any linear-Gaussian model such as (13)), for which the graph girth is guaranteed to be at least 6 and the degree of the function nodes is at most 2. This allows the application of the exact SPA computation at the nodes and

a high degree of parallelization, such that the resulting MP-based detector is very computationally efficient. Furthermore, the absence of cycles of length less than 6 yields good convergence properties of the SPA iterations.

We compare the proposed scheme with other three soft-output detectors proposed in the literature, namely: i) a different MP-based detector recently proposed in [25], based on an alternative way to construct the FG (see Section V-B); ii) a standard linear MMSE block equalizer, which offers very good performance at the impractical cost of a very large-dimensional matrix inversion; iii) a low-complexity MMSE block equalizer recently proposed in [32] that uses drastic simplifying assumptions (in particular, the bi-orthogonality of the OTFS $g_{\rm tx}$ and $g_{\rm rx}$ pulses and the assumption that the delay and Doppler shifts as integer multiples of the receiver sampling grid) such that the resulting *nominal* channel matrices $\boldsymbol{\Psi}_p$ are block-circulant with circulant blocks and the matrix inversion in linear MMSE estimation can be efficiently implemented. As we shall see, since these simplifying assumptions are not verified in practice (shifts are not on a quantized grid, and bi-orthogonal pulses with unit time-frequency product cannot exist [36]), the performance of this low-complexity linear detector is quite poor, when applied to a realistic channel and pulse scenario.

### *A. Proposed MP-based detector ("Matrix $\boldsymbol{G}$ algorithm" — $\mathrm{MP}_{\boldsymbol{G}}$)*

From (13), when $\boldsymbol{\Psi}$ is known (perfect CSI) and $\boldsymbol{w}$ is complex Gaussian independent and identically distributed (i.i.d.), the conditional probability density function (pdf) of the received samples $\boldsymbol{y}$ given the modulation symbols $\boldsymbol{x}$ is given by

$$p\left(\boldsymbol{y}|\boldsymbol{x}\right) = \frac{1}{\left(2\pi\sigma_w^2\right)^{-NM}} \exp\left(-\frac{\left\|\boldsymbol{y}-\boldsymbol{\Psi}\boldsymbol{x}\right\|^2}{2\sigma_w^2}\right) \propto \exp\left(-\frac{\left\|\boldsymbol{y}-\boldsymbol{\Psi}\boldsymbol{x}\right\|^2}{2\sigma_w^2}\right), \quad (37)$$

where the proportionality operator removes an irrelevant constant factor independent of symbols $\boldsymbol{x}$. We follow the FG construction approach of [31] and expand the $\ell_2$-norm inside the exponential as

$$\left\|\boldsymbol{y}-\boldsymbol{\Psi}\boldsymbol{x}\right\|^2 = \boldsymbol{y}^H\boldsymbol{y} - 2\mathrm{Re}\left\{\boldsymbol{x}^H\boldsymbol{\Psi}^H\boldsymbol{y}\right\} + \boldsymbol{x}^H\boldsymbol{\Psi}^H\boldsymbol{\Psi}\boldsymbol{x}. \quad (38)$$

Defining $\boldsymbol{z} \triangleq \boldsymbol{\Psi}^H\boldsymbol{y}$ and $\boldsymbol{G} \triangleq \boldsymbol{\Psi}^H\boldsymbol{\Psi}$, the conditional pdf can be written as

$$p\left(\boldsymbol{y}|\boldsymbol{x}\right) \propto \exp\left(\frac{2\mathrm{Re}\left\{\boldsymbol{x}^H\boldsymbol{z}\right\} - \boldsymbol{x}^H\boldsymbol{G}\boldsymbol{z}}{2\sigma_w^2}\right). \quad (39)$$

Note that the sequence $\boldsymbol{z}$ is a sufficient statistic for symbols detection. By expressing the matrix operations explicitly in terms of their components, we define the functions

$$F_i\left(x_i\right) \triangleq \exp\left[\frac{1}{\sigma_w^2}\mathrm{Re}\left\{z_i x_i^* - \frac{G_{i,i}}{2}\left|x_i\right|^2\right\}\right], \quad (40)$$

$$I_{i,j}\left(x_i, x_j\right) \triangleq \exp\left[-\frac{1}{\sigma_w^2}\mathrm{Re}\left\{G_{i,j}x_j x_i^*\right\}\right], \quad (41)$$

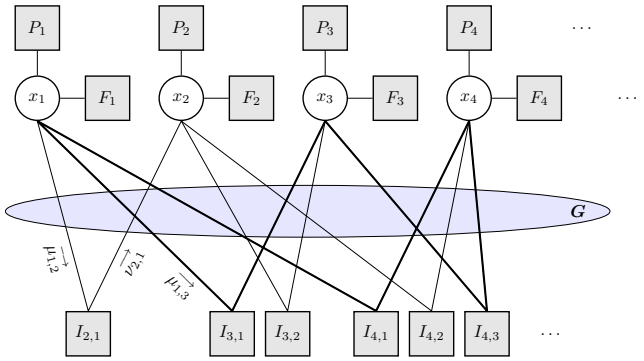


Fig. 2. Partial structure of the FG for the $\mathrm{MP}_{\boldsymbol{G}}$ algorithm.

and we use the Bayes rule in order to express the a-posteriori probability of $\boldsymbol{x}$ given $\boldsymbol{y}$ in the factored form, i.e.,

$$P\left(\boldsymbol{x}|\boldsymbol{y}\right) \propto P\left(\boldsymbol{x}\right) p\left(\boldsymbol{y}|\boldsymbol{x}\right) \propto \prod_{i=1}^{NM}\left[P\left(x_i\right) F_i\left(x_i\right) \prod_{j<i} I_{i,j}\left(x_i, x_j\right)\right], \quad (42)$$

where we used the fact that the modulation symbols $x_i$ take on values in some signal constellation $\mathcal{C}$ and are treated by the detector as i.i.d. with given (typically uniform) a-priori probability mass function $\{P(x) : x \in \mathcal{C}\}$.

In the proposed approach, the FG corresponds to the factorization in (42) (see the example shown in Fig. 2). At this point, the resulting MP-based soft-output detector follows immediately by applying the standard SPA computation rules. The detailed derivation of the message computation at the function and variable nodes of the FG is given in [31] and applies directly to our setting. Here, for the sake of completeness, we just summarize the resulting algorithm. First, define $V_i\left(x_i\right)$ as the product of all messages incoming to the variable node $x_i$, namely

$$V_i\left(x_i\right) \triangleq P_i\left(x_i\right) F_i\left(x_i\right) \prod_{j\neq i} \nu_{i,j}\left(x_j\right), \quad (43)$$

which is proportional to the (estimated) a-posteriori probability $P\left(x_i|\boldsymbol{y}\right)$ and thus provides the soft-output of the this detector. Then, the application of the SPA leads to the following rules for message exchange and update:

1) Computation at the variable nodes: each node $x_i$ sends to each adjacent function node $I_{i,j}$ the message

$$\mu_{i,j}\left(x_i\right) = V_i\left(x_i\right) / \nu_{i,j}\left(x_i\right). \quad (44)$$

2) Computation at the function nodes: each function node $I_{i,j}$ sends to each adjacent variable node $x_i$ the message

$$\nu_{i,j}\left(x_i\right) = \sum_{x_j\in\mathcal{C}} I_{i,j}\left(x_i, x_j\right) \mu_{i,j}\left(x_j\right). \quad (45)$$

Notice that all the variable nodes and the function nodes can be activated in alternative rounds and, in each round, all the nodes of the same type can be activated in parallel, e.g., adopting the same flooding schedule used for low-density parity check (LDPC) decoding [45]. Moreover, messages can be implemented in the logarithmic domain [37].

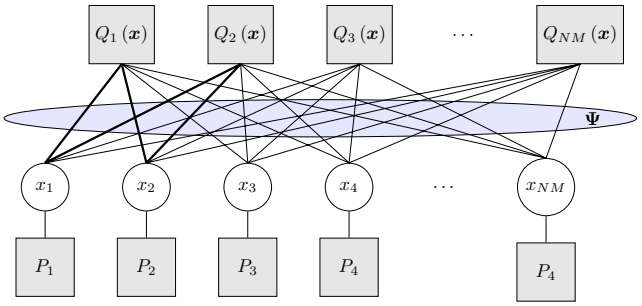


Fig. 3. Structure of the FG for the $\mathrm{MP}_{\boldsymbol{\Psi}}$ algorithm.

With the help of Fig. 2, we can illustrate some important features of the proposed approach.

i) FG of girth 6: the FG constructed as above is guaranteed to have girth (minimum length of cycles) equal to 6 (highlighted in bold in Fig. 2). It is well-known that the SPA yields exact posterior marginalization for cycle-free FGs, and the rationale behind the use of the SPA paradigm on loopy graphs is that if the FG has large girth, the local neighborhood of each node is "tree-like" [37]. In particular, cycles of length 4 should be avoided. Hence, the proposed construction following the general method of [31] yields indeed a FG better suited to the application of the iterative SPA.

ii) Computational complexity: notice that the computation in (41) involves the summation w.r.t. only a single discrete variable over the constellation $\mathcal{C}$. Therefore, this computation has always linear complexity in the constellation size, irrespectively on the sparsity of the channel matrix $\boldsymbol{\Psi}$. This allows the use of the exact SPA at fixed complexity per node, unlike the approach in [25] (see comments in Section V-B).

iii) High degree of parallelization: the number of nodes of type $I_{i,j}$ depends on the number of non-zero elements in the rows of the upper triangular part of the matrix $\boldsymbol{G}$ (the existence of edges is evidenced by the shadowed elliptic area in Fig. 2). Nevertheless, as said before, these degree-2 nodes $I_{i,j}$ can be all activated in parallel. Hence, for a sufficiently large degree of parallelization, the computational *time complexity* is independent of the sparsity of the multipath channel. Notice that in modern LDPC decoding is not unlikely to find implementations with degree of parallelization of the order of 1000, which is much larger than what needed in our detector. Hence, we claim that the proposed detector is very attractive from a practical implementation viewpoint.

### *B. MP-based algorithm of [25] ("Matrix $\boldsymbol{\Psi}$ algorithm" — $\mathrm{MP}_{\boldsymbol{\Psi}}$)*

The MP-based algorithm of [25] builds its FG from the more "direct" factorization of the a-posteriori probability

$$P(\boldsymbol{x}|\boldsymbol{y}) \propto P(\boldsymbol{x})\, p(\boldsymbol{y}|\boldsymbol{x}) = \prod_{i=1}^{N\times M} p(y_i|\boldsymbol{x}) \prod_{i=1}^{N\times M} P(x_i)\,. \quad (46)$$

Defining the function nodes

$$Q_i(\boldsymbol{x}) \triangleq p(y_i|\boldsymbol{x}) = \exp\left(\frac{\|y_i - \boldsymbol{\Psi}_i \boldsymbol{x}\|^2}{2\sigma_w^2}\right), \quad (47)$$

where $\boldsymbol{\Psi}_i$ is the $i$-th row of $\boldsymbol{\Psi}$, the resulting FG is shown in Fig. 3. Since the elements of the same $i$-th column $\boldsymbol{\Psi}$ are multiplied by the same symbol $x_i$, this FG has necessarily length-4 cycles (highlighted in bold in Fig. 3). The edges evidenced by the shadowed elliptic area in the figure correspond to the non-zero elements of the matrix $\boldsymbol{\Psi}$. In particular, the degree $d_i$ of the function node $Q_i(\boldsymbol{x})$ is equal to the number of non-zero elements in the $i$-th row $\boldsymbol{\Psi}_i$. The exact SPA computation at such function nodes requires summing over $d_i - 1$ discrete variables taking values in $\mathcal{C}$. Therefore, it has complexity $|\mathcal{C}|^{d_i-1}$ that may be prohibitively large for large constellations and, above all, it depends on the sparsity of the channel. Therefore, the exact application of the SPA computation rules to the FG obtained directly from the matrix $\boldsymbol{\Psi}$ is highly impractical. For this reason, the authors of [25] propose to use a Gaussian approximation of the interfering symbols in the computation at the nodes $Q_i(\boldsymbol{x})$, which effectively boils down to a soft interference cancellation approach, as already widely used in turbo equalization and pioneered in the context of multiuser detection in [46], [47]. For the sake of space limitation, we omit the details of the resulting MP algorithm, which can be found in [25].

It should also be mentioned that, for the sake of simplicity and in order to increase the sparsity of the FG in Fig. 3, the detector proposed in [25] constructs the *nominal* matrix $\boldsymbol{\Psi}$ by rounding the delay shifts to integers on receiver sampling grid. Under this condition, the channel matrix is very sparse since many coefficients corresponding to sampling at non-integer delay shifts are identically to zero, and the number of connections for each node is reduced, while preserving the length-4 cycles problem, unavoidable with this approach. Nevertheless, since the assumption is generally not satisfied by real-world channels, such approximation of the channel matrix results in neglecting a significant component of the ISI. We shall verify that when such integer delay shift rounding is applied to the construction of the nominal matrix $\boldsymbol{\Psi}$ used by the detector but the actual delay shifts have a fractional component (as it is always the case in practice), the *mismatch* yields a significant performance degradation. This shows that neglecting the fractional part of delays and Doppler shifts, as routinely done in the literature of OTFS, may be indeed quite misleading.

### *C. Linear block-wise MMSE equalization*

As a further term of comparison we consider also the standard linear MMSE block equalizer, applied to the channel model (13). In this case, the soft-output is simply the linear MMSE estimate of symbols $\boldsymbol{x}$ from the observation $\boldsymbol{y}$, given by

$$\hat{\boldsymbol{x}}_{\mathrm{LMMSE}} = \boldsymbol{\Psi}^H \left(\boldsymbol{\Psi}\boldsymbol{\Psi}^H + \sigma_w^2 \boldsymbol{I}\right)^{-1} \boldsymbol{y}\,. \quad (48)$$

The complexity of this approach is proportional to $\mathcal{O}\left((NM)^3\right)$, so it becomes quickly unfeasible for typical

TABLE I
SIMULATION PARAMETERS

| | |
|---|---|
| $f_c = 5.89$ GHz | $M = 64$ |
| $B = 10$ MHz | $N = 50$ |
| $\Delta f = B/M = 156.25$ kHz | $T = 1/\Delta f = 6.4\,\mu s$ |
| $\sigma_{\rm rcs} = 1$ m$^2$ | $G = 100$ |
| $r = 20$ m | $v = 80$ km/h |

values of $N$ and $M$ (e.g., in our simulations we have considered $N = 50$ and $M = 64$). A low-complexity (mismatched) linear minimum mean square error (LMMSE) approach was recently proposed in [32]. This relies on the cyclic properties of channel matrix $\boldsymbol{\Psi}$ under perfect bi-orthogonality of the modulation pulses $g_{\rm tx}$ and $g_{\rm rx}$ and integer-grid valued delays and Doppler shifts. As a result, in the presence of practical rectangular pulses and non-integer delays and Doppler shifts, as realistically considered in our work, the performance of this approach visibly degrades.

## VI. Simulation Results

The radar (backscattered) and forward communication SNRs have been defined in (2). In the case of multipath, we fix $\mathrm{SNR}_{\rm com}$ to be the SNR of the LoS component, and we add multipath components with progressively lower SNRs, such that the sum SNR of the channel increases with the number of paths $P$. This corresponds to the physically meaningful case that a richer propagation environment conveys more signal power. Table I summarizes the relevant simulation parameters inspired by the automotive communication standard IEEE 802.11p [11], where $r$ and $v$ denote the target range and velocity.

### A. Comparison with OFDM and FMCW

We briefly review OFDM and the widely used radar waveform known as FMCW [40, Chapter 4.6]. For both OFDM and FMCW we consider a symbol length of $T_0 = T_{\rm GI} + T$ including a guard interval denoted by $T_{\rm GI}$, longer than the maximum path delay $\tau_{\max}$. In OFDM, the CP length is given by $T_{\rm GI} = C\frac{T}{M}$, with $C = \lceil \frac{\tau_{\max}}{T/M} \rceil$. We send $NM$ modulation symbols $\{x_{n,m}\}$ in the time-frequency domain, satisfying the average power constraint (3). The OFDM receiver samples at rate $T/M$ and removes the CP before detection in order to eliminate the inter-symbol interference. For the case of a single path channel ($P = 1$), the ML estimator and the related CRLB can be found in our related work [28] and are omitted here for the sake of space limitation.

In FMCW, the radar transmitter sends a sequence of identical "chirp" pulses of duration $T$, each followed by a guard interval of length $T_{\rm GI}$ to avoid inter-pulse interference. By letting $\phi(t) = (f_c + \frac{B}{2T}t)t$ denotes the phase at time $t$, the transmit signal is given by

$$s\left(t\right) = \sum_{i=0}^{N-1} e^{j2\pi\phi(t-iT_0)} \mathrm{rect}\left(\frac{t-iT_0}{T}\right), \tag{49}$$

where we consider $N$ pulses to make a fair comparison with OFDM. Plugging (49) into (6) , we obtain the received signal $r(t)$, by neglecting the noise. After some algebra, it is easy to show that the product of the received and the transmit signals gives

$$y(t) = r(t)s^*(t) = \sum_{p=0}^{P-1} h_p e^{j2\pi\nu_p t} e^{-j2\pi f_c \tau_p} \times \sum_{i=0}^{N-1} e^{-j2\pi f_{b,p}(t-iT_0-\tau_p/2)}, \tag{50}$$

where we let $f_{b,p} = \frac{B}{T}\tau_p$ denotes the so-called *beating frequency* of path $p$. The receiver samples $y(t)$ every $T/M$ for each pulse, i.e., for $t = iT_0 + l\frac{T}{M}$ where $i$ denotes the pulse index and $l$ denotes the sample index. By letting $L = M + C$ denotes the number of samples per pulse, the sampled received signal can be rewritten as

$$y[i,l] \triangleq y\left(iT_0 + \frac{l}{f_s}\right) = \sum_p h_p e^{j2\pi(f_{b,p}+\nu_p)\frac{l}{f_s}} e^{j2\pi\nu_p iT_0}, \tag{51}$$

for $i = 0, \ldots, N-1$ and $l = 0, \ldots, L-1$, where $h_p$ absorbs a constant phase term independent of the indices $i, l$.

The estimation of the $2P$ unknown parameters $\{\tau_p, \nu_p\}$ is thus obtained by selecting the peak of the range-Doppler map found by applying a two-dimensional discrete Fourier transform (DFT) to the noisy samples in (51) as proposed in [10], [18]. The range and velocity of the target are obtained by the estimates of $\{\tau_0, \nu_0\}$.

### B. Joint Radar and Communication Performance

The first two subfigures of Fig. 4 show the velocity and range estimation root MSE (RMSE) versus $\mathrm{SNR}_{\rm rad}$ for a pure LoS channel ($P = 1$) and for OTFS, OFDM, and FMCW. We notice that both digital modulation formats provide as accurate radar performance as FMCW, while transmitting at their full information rate. It is remarkable to note that the combination of the waterfall analysis and the CRLB introduced in Section IV-B is able to accurately predict the actual ML estimation performance.

In addition, the third subfigure of Fig. 4 shows the achievable rate with Gaussian independent and i.i.d. symbols $C_{\rm Gauss}$, which provides an achievable rate in the case of *joint detection and decoding* (with unconstrained complexity), as a function of $\mathrm{SNR}_{\rm com}$. Given the fact that we can model the input-output OTFS block channel as a MIMO channel, the mutual information with Gaussian inputs and perfect CSI at the receiver is given by [48]

$$C_{\rm Gauss}^{\rm OTFS} = \frac{NT}{NT + T_{\rm GI}} \frac{1}{NM} \log_2 \det\left(\boldsymbol{I} + \mathrm{SNR}_{\rm com}\boldsymbol{\Psi}\boldsymbol{\Psi}^H\right). \tag{52}$$

An analogous expression for OFDM, owing to the fact that the channel matrix in OFDM is diagonal, yields

$$C_{\rm Gauss}^{\rm OFDM} = \frac{T}{T + T_{\rm GI}} \log_2\left(1 + \mathrm{SNR}_{\rm com}\right). \tag{53}$$

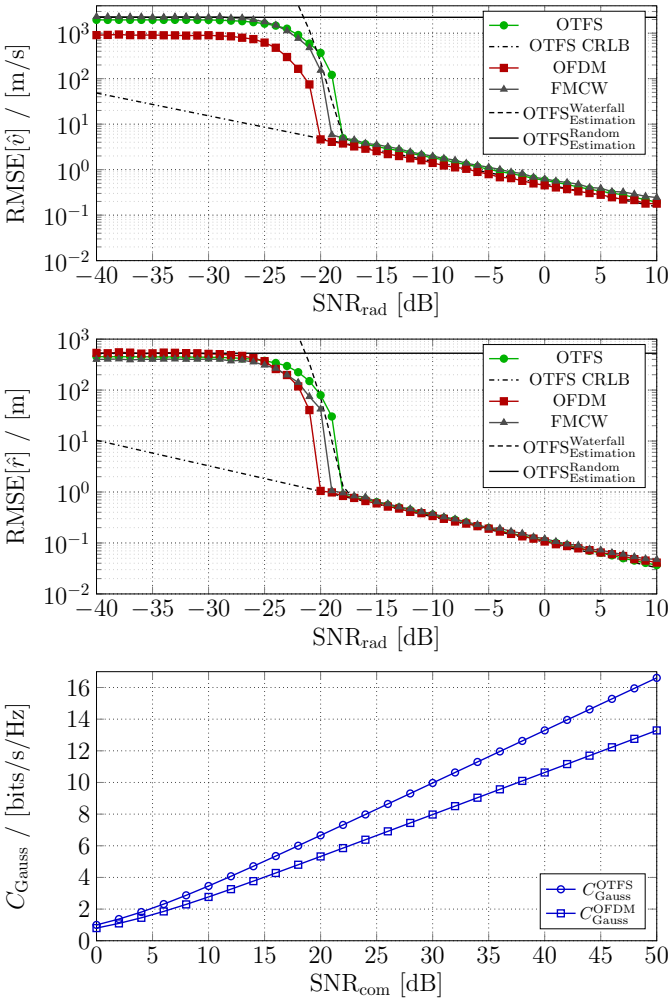


Fig. 4. From top to bottom: the RMSE of the target velocity estimation $\hat{v}$ vs $\text{SNR}_{\text{rad}}$, the RMSE of the target range estimation $\hat{r}$ vs $\text{SNR}_{\text{rad}}$, and the Gaussian capacity $\mathcal{C}_{\text{Gauss}}$ vs. $\text{SNR}_{\text{com}}$, for the curves indicated in the different legends.

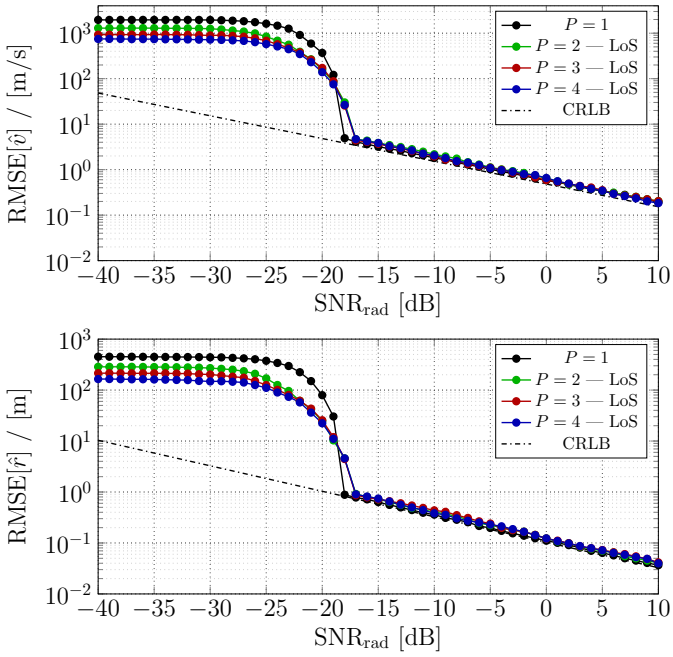


Fig. 5. RMSE of the target velocity estimation $\hat{v}$ vs $\text{SNR}_{\text{rad}}$ and range estimation $\hat{r}$ vs $\text{SNR}_{\text{rad}}$ for a multipath channel ($P \in [1, 2, 3, 4]$).

The factors $\frac{NT}{NT+T_{\text{GI}}}$ and $\frac{T}{T+T_{\text{GI}}}$ for OTFS and OFDM, respectively, are introduced in order to take into account the insertion of the guard interval. In OTFS, a guard interval of duration $T_{\text{GI}}$ is inserted at the end of each frame of duration $NT$, comprising $N$ symbols in the time domain. In contrast, in OFDM, the guard interval in the form of CP is inserted at each OFDM symbol of duration $T$. It is clear that for practical values of the OTFS frame length $N$, the overhead paid by OTFS is much less than the CP overhead paid by OFDM (in these results we used $T_{\text{GI}} = T/4$, which is typical in the IEEE 802.11 family of standards). On the other hand, the larger overhead incurred by OFDM yields a particularly simple receiver structure, since the channel matrix is diagonalized. In contrast, as we have seen extensively in this paper, OTFS requires block-wise detection over the whole frame, which can be very computationally intensive. This is why the proposed soft-output symbol detector presented in Section V-A is of particular interest, as it will be demonstrated by the results of the next subsection.

Next, we present a second set of results where we consider only OTFS in the presence of multipath channels ($P > 1$, up to $P = 4$) and show the effectiveness of our proposed approximated ML parameter estimator with at most 5 iterations, under the assumption that paths are spaced enough in the Doppler-delay grid. In our analysis, we suppose that the number of paths, as well as the presence of the target in the beam sector analyzed, is known at the radar receiver. In Fig. 5 we show the range and velocity RMSE in a multipath scenario, where the parameters of interest are those of the LoS path. As expected, the performance slightly degrades as the number of paths increases, but such degradation is very mild, showing the robustness of the proposed joint parameter estimation method. Notice also that the CRLB is plotted for the case $P = 1$ only.

### C. Performance of Separated Detection and Decoding

As already mentioned, we characterize the performance of separated detection and decoding schemes in terms of pragmatic capacity, i.e., the mutual information of the virtual channel with input the constellation symbols used with uniform probability and output provided by the soft-output of the detector. This mutual information provides an achievable rate for separated detection and decoding for a given detection scheme [29], [30].

Let us consider a sequence of $NM$ symbols $\{x_k\}$ belonging to the signal constellation $\mathcal{C}$, and let $V_k(x_k)$ denotes the detector soft-output. In the case of MP-based detectors, $V_k(x_k)$ is given in the form of a posterior probability distribution on $x_k \in \mathcal{C}$, while in the case of linear equalizers (e.g., the linear MMSE estimator in (48)), this is given as the noisy estimate $\hat{x}_k$ which is treated as the output of a (virtual) AWGN channel. In any case, the pragmatic capacity is simply defined as the symbol-by-symbol mutual information $I_{\text{PC}}(x_k; V(x_k))$. When $V(x_k)$ takes on the form of a posterior probability

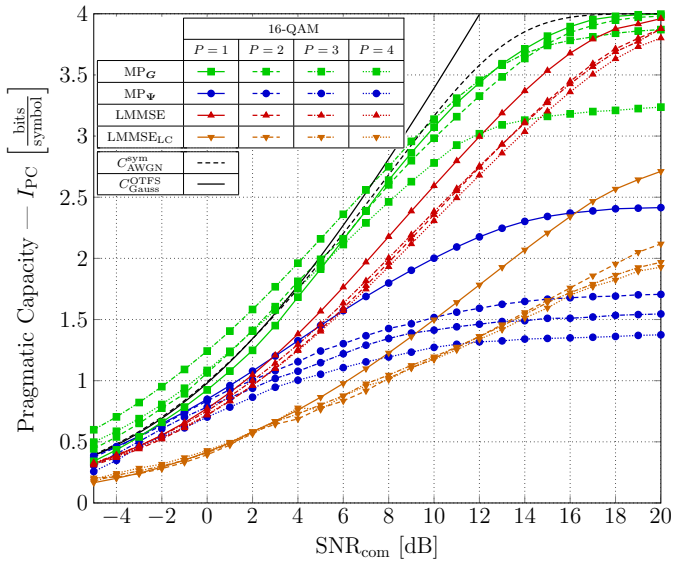


Fig. 6. Symbols detection performance in terms of pragmatic capacity for 16-QAM modulation. The curves show the behavior of matrix $\boldsymbol{G}$ based MP algorithm and MP algorithm of [25] under approximated channel conditions, i.e., with delay and Doppler shifts on the Doppler-delay grid, for a multipath channel with different number of components $P$.

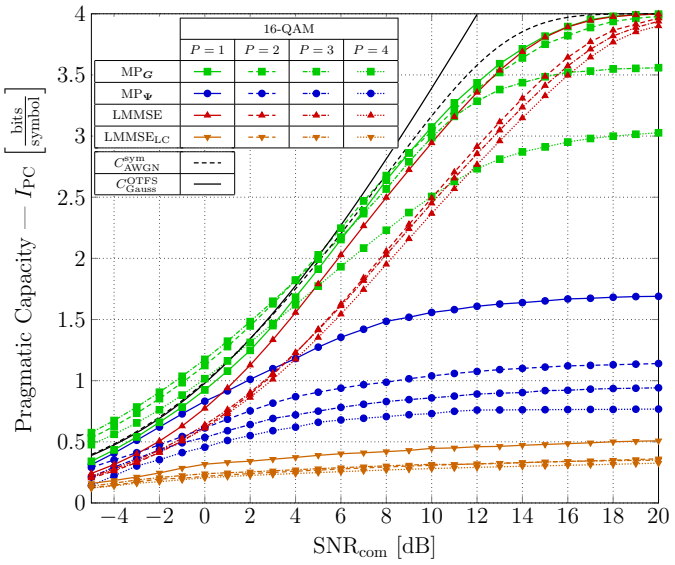


Fig. 7. Symbols detection performance in terms of pragmatic capacity for 16-QAM modulation. The curves show the behavior of matrix $\boldsymbol{G}$ based MP algorithm and MP algorithm of [25] under real channel conditions, i.e., with delay and Doppler shifts not on the Doppler-delay grid, for a multipath channel with different number of components $P$.

distribution, this can be easily calculated by Monte Carlo simulation via the formula

$$I_{\text{PC}}(x_k;V(x_k)) \triangleq H(x_k) - H(x_k|V(x_k)) = \log_2 \mathcal{C} - E\left\{\sum_{x_k\in\mathcal{C}} V(x_k)\log_2\frac{1}{V(x_k)}\right\}, \quad (54)$$

where the expectation is obtained by Monte Carlo simulations from the detector output. In the case of linear equalization (i.e., $V(x_k)=\hat{x}_k$), the pragmatic capacity is simply given by the *symmetric capacity* (i.e., with symbols used with uniform probability) of the signal constellation $\mathcal{C}$, for an AWGN channel with SNR equal to the output signal-to-interference noise ratio (SINR) of the equalizer. For the sake of comparison, we also show the symmetric capacity of the signal constellation in an AWGN channel with SNR equal to $\text{SNR}_{\text{com}}$ (i.e., the SNR of the LoS path), denoted by $C^{\text{sym}}_{\text{AWGN}}$, and the mutual information with Gaussian inputs $C^{\text{OTFS}}_{\text{Gauss}}$, for the case $P=1$.

Fig. 6 and Fig. 7 show the performance of the various methods for OTFS soft-output detection considered in Section V for a 16-quadrature amplitude modulation (QAM). Fig. 6 shows the results for the (unrealistic) case where the channel Doppler shifts and delays are exactly on the discrete Doppler-delay grid used by the receiver sampling. In contrast, Fig. 7 shows the results when the actual channel has arbitrary Doppler and delay shifts (with a random uniformly distributed fractional part), but certain algorithms *assume* such integer grid when constructing the nominal channel matrix $\boldsymbol{\Psi}$ used by the detector (as advocated for example in [25]).

We notice that the proposed MP-based approach outperforms the one in [25] in both cases. In particular, it suffers from almost no degradation due to the non-integer Doppler and delay shifts, unlike the method of [25]. The LMMSE equalizer (48) with full complexity yields very good performance, paying only a small SNR penalty with respect to the proposed MP-based scheme for $P=1,2$, and outperforming the MP-based scheme for richer scattering $P=3,4$. However, as said before, its complexity is cubic in the frame dimension $NM$, which is unaffordable in practical implementations. Unfortunately, the low-complexity LMMSE estimator (curves indicated by $\text{LMMSE}_{\text{LC}}$ in the figures) of [32] exploits a specific structure of the channel matrix $\boldsymbol{\Psi}$. The required doubly block circulant feature of the OTFS channel matrix, as defined in [32], is satisfied only when $g_{\text{tx}}$ and $g_{\text{rx}}$ are bi-orthogonal. Under such condition, the scheme proposed in [32] coincides with the MMSE block equalizer without the need of a large matrix inversion. In our model, we adopted physically realizable and realistic rectangular pulses, which clearly do not satisfy the bi-orthogonal condition. As a consequence, the doubly block circulant feature is lost. Our simulations show that the approach [32] is not competitive when applied to a channel model using rectangular pulses. It should be noticed that bi-orthogonality for pulses with time-frequency product equal to 1 is mathematically impossible [36]. Hence, relaying on such assumption may be very misleading, as shown by our results.

Note that, due to the space limitation, we only treat a 16-QAM modulation. However, the results are very clear and plots with different modulation formats would have only been a confirmation of what we stated above.

## VII. Conclusions

We studied a joint radar parameter estimation and communication system based on the OTFS modulation format, over a time-frequency selective channels formed by discrete multipath components, each of which is characterized by a complex amplitude, a Doppler shift, and a delay. The radar parameters of interest are the delay and the Doppler shift of the shortest path (assumed to be in LoS propagation), related

$$\boldsymbol{\Psi}^{p}_{k,k'}[l,l'] = \frac{1}{NM}\sum_{n,n',m,m'} e^{j2\pi n' T\nu_p} e^{-j2\pi m\Delta f\tau_p} e^{-j2\pi\left(\frac{nk}{N}-\frac{ml}{M}-\frac{n'k'}{N}+\frac{m'l'}{M}\right)} \times \frac{T}{M}\sum_{i=0}^{M-1} g_{\mathrm{tx}}\left(i\frac{T}{M}\right) g^{*}_{\mathrm{rx}}\left(i\frac{T}{M}-(n-n')T+\tau_p\right) e^{-j2\pi\left((m-m')\Delta f+\nu_p\right)i\frac{T}{M}} \tag{55}$$

$$\boldsymbol{\Psi}^{p}_{k,k'}[l,l'] = \frac{T}{NM}\sum_{n,n',m} e^{j2\pi(n'T\nu_p-m\Delta f\tau_p)} e^{-j2\pi\left(\frac{nk}{N}-\frac{ml}{M}-\frac{n'k'}{N}\right)} g_{\mathrm{tx}}\left(l'\frac{T}{M}\right) g^{*}_{\mathrm{rx}}\left(l'\frac{T}{M}-(n-n')T+\tau_p\right) e^{-j2\pi(m\Delta f+\nu_p)l'\frac{T}{M}} \tag{58}$$

$$\boldsymbol{\Psi}^{p}_{k,k'}[l,l'] = \frac{T}{NM}\left(\sum_{m} e^{j2\pi\left(l-M\Delta f\tau_p-l'\right)\frac{m}{M}}\right) e^{-j2\pi\nu_p l'\frac{T}{M}} \left(\sum_{n} e^{j2\pi\left(NT\nu_p+k'-k\right)\frac{n}{N}}\right) \times\left\{ g_{\mathrm{tx}}\left(l'\frac{T}{M}\right) g^{*}_{\mathrm{rx}}\left(l'\frac{T}{M}+\tau_p\right) + g_{\mathrm{tx}}\left(l'\frac{T}{M}\right) g^{*}_{\mathrm{rx}}\left(l'\frac{T}{M}-T+\tau_p\right) e^{-j2\pi\frac{k'+\nu_p NT}{N}}\right\} \tag{59}$$

to the range and velocity of the target. We derived an efficient approximated ML parameter estimation scheme as well as bounds and tight approximations on the estimation MSE of the radar detector. The proposed estimation scheme for OTFS provides as accurate estimation as state-of-the art dedicated radar waveforms such as FMCW, while the digitally modulated signal is used to transmit information at full rate (i.e., all symbols are coded information symbols). This show that joint radar parameter estimation and data communication can be achieved with virtually no penalty for each of the functions, at the only cost of complexity of the radar detector, which is significantly more complicated than the corresponding detector for FMCW.

We also considered a practical low-complexity soft-output detector for OTFS separated detection and decoding based on message passing, derived by applying the canonical SPA computation rules to a particular realization of the FG of the underlying joint posterior probability distribution of the modulation symbols given the received signal frame. The proposed MP-based soft-output detector shows very good performance at low complexity (especially because it is suitable for a highly parallelized implementation). In particular, the proposed scheme outperforms other recently proposed MP-based schemes, and provides a competitive performance/complexity tradeoff with respect to the block-wise linear MMSE detector, which is prohibitively complex. As such, the proposed detector represents the new state-of-the-art for OTFS soft-output detection. An interesting issue for future work is to investigate the performance of "Turbo Equalization", when the soft-output detector is iteratively re-processed using the soft-ouptut of an outer channel decoder. Our proposed scheme appears to be ideally suited and easily adapted to such Turbo Equalization schemes.

## VIII. Acknowledgment

The work of Lorenzo Gaudio, Giuseppe Caire, and Giulio Colavolpe is supported by Fondazione Cariparma, under the TeachInParma Project. The work of Mari Kobayashi is supported by an Alexander von Humboldt Research Fellowship. This research benefits from the HPC (High Performance Computing) facility of the University of Parma, Italy. The authors would like to thank Björn Bissinger for his support on an early version of this paper.

## Appendix

Here, we show the mathematical derivation of (15) starting from (12). By substituting in (12) the approximated cross-ambiguity function in (14), we get (55). By expressing the Dirichlet kernel as

$$\sum_{z=0}^{Z-1} e^{j2\pi\phi\frac{z}{Z}} = \frac{e^{j2\pi\phi}-1}{e^{j2\pi\phi/Z}-1}\,, \tag{56}$$

whose value for $\phi\in\mathbb{N}$ is $\neq 0$ if and only if $\phi=0$, it readily follows that the sum w.r.t. $m'$, which can be taken out all other summations, is

$$\sum_{m'} e^{-j2\pi\left(l'-i\right)\frac{m'}{M}} = M\delta\left(l'-i\right)\,. \tag{57}$$

Thus, exploiting the delta function, i.e., by setting $i=l'$, we get (58). At this point, as already said, by letting $g_{\mathrm{tx}}(t)$ and $g_{\mathrm{rx}}(t)$ be rectangular pulses of length $T$, by limiting the channel delay to $\tau_{\max}<T$, it readily follows that the multiplication of $g_{\mathrm{tx}}(t)$ and $g_{\mathrm{rx}}(t)$ yields non-zero samples only for $n'=n$ and $n'=n-1$, which limits the summation w.r.t. $n'$ to two terms only. Thus, exploiting this fact and reordering the summations we obtain (59), where we used $\Delta fT=1$. Note that the multiplication between the rectangular pulses $g_{\mathrm{tx}}$ and $g_{\mathrm{rx}}$ involves mutually exclusive $l'$, since it considers the overlap between the pulses in the intervals $[0, M-1-M-1-\lceil\tau_i/(T/M)\rceil]$ and $[M-1-\lfloor\tau_i/(T/M)\rfloor, M-1]$ (note that one of the two multiplications has an additional delay of $-T$ for pulse $g_{\mathrm{rx}}$). This behavior can be easily seen by drawing the two pulses, and a more detailed analysis can be found in [25]. Thus, given $g^{*}_{\mathrm{rx}}(t)\,g_{\mathrm{tx}}(t)=1/T$, by expressing the remaining summations as Dirichlet kernels, we finally get (15).

## REFERENCES


[1] L. Zheng, M. Lops, Y. C. Eldar, and X. Wang, "Radar and communication co-existence: an overview: a review of recent methods," *IEEE Signal Process. Mag.*, vol. 36, no. 5, pp. 85–99, Sep. 2019.

[2] S. Chen, J. Hu, Y. Shi, Y. Peng, J. Fang, R. Zhao, and L. Zhao, "Vehicle-to-everything (V2X) services supported by LTE-based systems and 5G," *IEEE Communications Standards Magazine*, vol. 1, no. 2, pp. 70–76, 2017.

[3] G. Hakobyan and B. Yang, "High-performance automotive radar: A review of signal processing algorithms and modulation schemes," *IEEE Signal Process. Mag.*, vol. 36, no. 5, pp. 32–44, 2019.

[4] G. R. Muns, K. V. Mishra, C. B. Guerra, Y. C. Eldar, and K. R. Chowdhury, "Beam alignment and tracking for autonomous vehicular communication using IEEE 802.11ad-based radar," in *IEEE INFOCOM 2019 - IEEE Conference on Computer Communications Workshops (INFOCOM WKSHPS)*, April 2019, pp. 535–540.

[5] E. Grossi, M. Lops, L. Venturino, and A. Zappone, "Opportunistic radar in IEEE 802.11ad networks," *IEEE Trans. Signal Process.*, vol. 66, no. 9, pp. 2441–2454, May 2018.

[6] E. Grossi, M. Lops, and L. Venturino, "Adaptive detection and localization exploiting the IEEE 802.11 ad standard," *arXiv preprint arXiv:1904.12835*, 2019.

[7] P. Kumari, J. Choi, N. González-Prelcic, and R. W. Heath, "IEEE 802.11ad-based radar: An approach to joint vehicular communication-radar system," *IEEE Trans. Veh. Technol.*, vol. 67, no. 4, pp. 3012–3027, April 2018.

[8] X. Song, S. Haghighatshoar, and G. Caire, "Efficient beam alignment for millimeter wave single-carrier systems with hybrid MIMO transceivers," *IEEE Trans. Wireless Commun.*, vol. 18, no. 3, pp. 1518–1533, March 2019.

[9] C. Sturm and W. Wiesbeck, "Waveform design and signal processing aspects for fusion of wireless communications and radar sensing," *Proc. IEEE*, vol. 99, no. 7, pp. 1236–1259, July 2011.

[10] S. M. Patole, M. Torlak, D. Wang, and M. Ali, "Automotive radars: A review of signal processing techniques," *IEEE Signal Process. Mag.*, vol. 34, no. 2, pp. 22–35, March 2017.

[11] D. H. N. Nguyen and R. W. Heath, "Delay and doppler processing for multi-target detection with IEEE 802.11 OFDM signaling," in *Proc. IEEE Int. Conf. Acoustics, Speech, and Signal Processing (ICASSP)*, March 2017, pp. 3414–3418.

[12] D. Ma, N. Shlezinger, T. Huang, Y. Liu, and Y. C. Eldar, "Joint radar-communications strategies for autonomous vehicles," *arXiv preprint arXiv:1909.01729*, 2019.

[13] S. H. Dokhanchi, M. B. Shankar, M. Alaee-Kerahroodi, T. Stifter, and B. Ottersten, "Adaptive waveform design for automotive joint radar-communications system," in *Proc. IEEE Int. Conf. Acoustics, Speech, and Signal Processing (ICASSP)*. IEEE, 2019, pp. 4280–4284.

[14] K. V. Mishra, M. R. Bhavani Shankar, V. Koivunen, B. Ottersten, and S. A. Vorobyov, "Towards millimeter wave joint radar-communications: A signal processing perspective," *IEEE Signal Process. Mag.*, vol. 36, no. 5, pp. 100–114, Sep. 2019.

[15] S. H. Dokhanchi, B. S. Mysore, K. V. Mishra, and B. Ottersten, "A mmWave automotive joint radar-communications system," *IEEE Trans. Aerosp. Electron. Syst.*, vol. 55, no. 3, pp. 1241–1260, June 2019.

[16] S. H. Dokhanchi, M. R. B. Shankar, T. Stifter, and B. Ottersten, "OFDM-based automotive joint radar-communication system," in *2018 IEEE Radar Conference (RadarConf18)*, April 2018, pp. 0902–0907.

[17] A. Hassanien, M. G. Amin, E. Aboutanios, and B. Himed, "Dual-function radar communication systems: A solution to the spectrum congestion problem," *IEEE Signal Process. Mag.*, vol. 36, no. 5, pp. 115–126, Sep. 2019.

[18] M. Braun, "OFDM radar algorithms in mobile communication networks," *Ph.D. Thesis at Karlsruhe Institute of Technology*, 2014.

[19] Y. Liu, G. Liao, J. Xu, Z. Yang, and Y. Zhang, "Adaptive OFDM integrated radar and communications waveform design based on information theory," *IEEE Commun. Lett.*, vol. 21, no. 10, pp. 2174–2177, 2017.

[20] P. Raviteja, K. T. Phan, Y. Hong, and E. Viterbo, "Orthogonal time frequency space (OTFS) modulation based radar system," *arXiv e-prints*, p. arXiv:1901.09300, Jan. 2019.

[21] M. Kobayashi, G. Caire, and G. Kramer, "Joint state sensing and communication: Optimal tradeoff for a memoryless case," in *Proc. IEEE Int. Symp. Inf. Theory*, June, 2018.

[22] K. Mahler, W. Keusgen, F. Tufvesson, T. Zemen, and G. Caire, "Measurement-based wideband analysis of dynamic multipath propagation in vehicular communication scenarios," *IEEE Trans. Veh. Technol.*, vol. 66, no. 6, pp. 4657–4667, 2016.

[23] ——, "Tracking of wideband multipath components in a vehicular communication scenario," *IEEE Trans. Veh. Technol.*, vol. 66, no. 1, pp. 15–25, 2016.

[24] R. Hadani, S. Rakib, A. F. Molisch, C. Ibars, A. Monk, M. Tsatsanis, J. Delfeld, A. Goldsmith, and R. Calderbank, "Orthogonal time frequency space (OTFS) modulation for millimeter-wave communications systems," in *2017 IEEE MTT-S International Microwave Symposium (IMS)*, June 2017, pp. 681–683.

[25] P. Raviteja, K. T. Phan, Y. Hong, and E. Viterbo, "Interference cancellation and iterative detection for orthogonal time frequency space modulation," *IEEE Trans. Wireless Commun.*, vol. 17, no. 10, pp. 6501–6515, Oct 2018.

[26] W. Shen, L. Dai, J.-p. An, P. Fan, and R. W. Heath, "Channel estimation for orthogonal time frequency space (OTFS) massive MIMO," *IEEE Trans. Signal Process.*, vol. 67, no. 16, pp. 4204–4217, Aug 2019.

[27] P. Raviteja, K. T. Phan, and Y. Hong, "Embedded Pilot-Aided Channel Estimation for OTFS in Delay-Doppler Channels," *IEEE Trans. Veh. Technol.*, vol. 68, no. 5, pp. 4906–4917, May 2019.

[28] L. Gaudio, M. Kobayashi, B. Bissinger, and G. Caire, "Performance analysis of joint radar and communication using OFDM and OTFS," in *Proc. IEEE Int. Conf. Commun.*, May 2019, pp. 1–6.

[29] A. Kavcic, Xiao Ma, and M. Mitzenmacher, "Binary intersymbol interference channels: Gallager codes, density evolution, and code performance bounds," *IEEE Trans. Inf. Theory*, vol. 49, no. 7, pp. 1636–1652, July 2003.

[30] J. B. Soriaga, H. D. Pfister, and P. H. Siegel, "Determining and approaching achievable rates of binary intersymbol interference channels using multistage decoding," *IEEE Trans. Inf. Theory*, vol. 53, no. 4, pp. 1416–1429, April 2007.

[31] G. Colavolpe, D. Fertonani, and A. Piemontese, "SISO detection over linear channels with linear complexity in the number of interferers," *IEEE J. Sel. Topics Signal Process.*, vol. 5, no. 8, pp. 1475–1485, Dec 2011.

[32] J. Cheng, H. Gao, W. Xu, Z. Bie, and Y. Lu, "Low-complexity linear equalizers for OTFS exploiting two-dimensional fast fourier transform," *arXiv preprint arXiv:1909.00524*, 2019.

[33] F. Athley, *Space-time parameter estimation in radar array processing*. Department of Signals and Systems, School of Electrical Engineering, Chalmers University of Technology., 2003.

[34] F. Athley, "Threshold region performance of maximum likelihood direction of arrival estimators," *IEEE Trans. Signal Process.*, vol. 53, no. 4, pp. 1359–1373, April 2005.

[35] A. Nimr, M. Chafii, M. Matthe, and G. Fettweis, "Extended GFDM framework: OTFS and GFDM comparison," in *Proc. IEEE Global Telecommun. Conf.*, Dec 2018, pp. 1–6.

[36] G. Matz, H. Bolcskei, and F. Hlawatsch, "Time-frequency foundations of communications: Concepts and tools," *IEEE Signal Process. Mag.*, vol. 30, no. 6, pp. 87–96, Nov 2013.

[37] F. R. Kschischang, B. J. Frey, and H. . Loeliger, "Factor graphs and the sum-product algorithm," *IEEE Trans. Inf. Theory*, vol. 47, no. 2, pp. 498–519, Feb 2001.

[38] A. Sabharwal, P. Schniter, D. Guo, D. W. Bliss, S. Rangarajan, and R. Wichman, "In-band full-duplex wireless: Challenges and opportunities," *IEEE J. Sel. Areas Commun.*, vol. 32, no. 9, pp. 1637–1652, Sep. 2014.

[39] G. A. Vitetta, D. P. Taylor, G. Colavolpe, F. Pancaldi, and P. A. Martin, *Wireless communications: algorithmic techniques*. John Wiley & Sons, 2013.

[40] M. A. Richards, *Fundamentals of radar signal processing, Second edition*. McGraw-Hill Education, 2014.

[41] L. Gaudio, M. Kobayashi, G. Caire, and G. Colavolpe, "Joint radar target detection and parameter estimation with mimo otfs," *arXiv preprint arXiv:2004.11035*, 2020.

[42] C. Cordeiro, D. Akhmetov, and M. Park, "IEEE 802.11 ad: Introduction and performance evaluation of the first multi-gbps WiFi technology," in *Proceedings of the 2010 ACM international workshop on mmWave communications: from circuits to networks*. ACM, 2010, pp. 3–8.

[43] D. R. Fuhrmann, E. J. Kelly, and R. Nitzberg, "A CFAR adaptive matched filter detector," *IEEE Trans. Aerosp. Electron. Syst.*, vol. 28, no. 1, pp. 208–216, 1992.

[44] M. Zhang, F. Wang, X. Yuan, and L. Chen, "2D structured turbo compressed sensing for channel estimation in OTFS systems," in *2018 IEEE International Conference on Communication Systems (ICCS)*, Dec 2018, pp. 45–49.

[45] T. J. Richardson and R. L. Urbanke, "The capacity of low-density parity-check codes under message-passing decoding," *IEEE Trans. Inf. Theory*, vol. 47, no. 2, pp. 599–618, Feb 2001.

[46] Xiaodong Wang and H. V. Poor, "Iterative (turbo) soft interference cancellation and decoding for coded CDMA," *IEEE Trans. Commun.*, vol. 47, no. 7, pp. 1046–1061, July 1999.
[47] J. Boutros and G. Caire, "Iterative multiuser joint decoding: unified framework and asymptotic analysis," *IEEE Trans. Inf. Theory*, vol. 48, no. 7, pp. 1772–1793, July 2002.
[48] E. Telatar, "Capacity of multi-antenna gaussian channels," *Europ J. Trans. Telecommun.*, vol. 10, no. 6, pp. 585–595, 1999.